Strathprints Institutional Repository

Shakedown analyses for rolling and sliding contact problems

H. F. Chen [*], Alan R.S. Ponter [*], G Specchia [°] and M Ciavarella [×]

[*] Department of Engineering, University of Leicester, Leicester, LE1 7RH, UK

e-mail: hfc3@le.ac.uk, asp@le.ac.uk

[°] Politecnic di Bari, Italy,

[° ×] CNT-ITC(Consiglio Nazionale delle Ricerche – 1st Tecnol. Costruz.), Bari, Italy

Abstract: There is a range of problems where repeated rolling or sliding contact occurs. For such problems shakedown and limit analyses provides significant advantages over other forms of analysis when a global understanding of deformation behaviour is required. In this paper, a recently developed numerical method. Ponter and Engelhardt (2000) and Chen and Ponter (2001), for 3-D shakedown analyses is used to solve the rolling and sliding point contact problem previously considered by Ponter, Hearle and Johnson (1985) for a moving Herzian contact, with friction, over a half space. The method is an upper bound programming method, the Linear Matching Method, which provides a sequence of reducing upper bounds that converges to the least upper bound associated with a finite element mesh and may be implemented within a standard commercial finite element code. The solutions given in Ponter, Hearle and Johnson (1985) for circular contacts are reproduced and extended to the case when the frictional contact stresses are at an angle to the direction of travel. Solutions for the case where the contact region is elliptic are also given.

Keywords: plasticity**,** limit loads, shakedown, Herzian contact

1. Introduction

The problem of the deformation of surfaces subjected to repeated rolling and sliding contact is a significant problem in number of areas of engineering design. For metallic surfaces rolling contact occurs in bearings and in the contact region of railway wheels and lines. The failure of such surfaces is often associated with the growth of strain near the contacted surface. A particularly effective way of gaining

insight into the combination of loads at which such strain growth initiates is to evaluate the loads corresponding to the shakedown limit for the problem, using the upper and lower bound shakedown theorems for an elastic perfectly plastic material.

Ponter Hearle and Johnson (1985) discussed the application of the upper bound shakedown theorem to such problems and showed that, for a von Mises yield condition, mechanism of deformation consisted of slip surfaces that surrounded the contact area and allowed a region of the surface to slide forward in the direction of travel of the rolling contact. Such mechanisms are capable of providing the exact solution under the assumption that the associated displacements, in the exact solution, were only in the direction of travel, i.e. there was no "ploughing" component to the deformation field. With this insight, it is then possible to calculate optimal upper bounds corresponding to the particular slip surface that produces the least upper bounds. The problem discussed by Ponter Hearle and Johnson (1985) is shown as Figure 1 where Hertzian contact pressure due to a normal load P is applied to a circular or elliptical region on a half space, together with a friction tangential force fP in the direction of travel of rolling contact. The contacting loads repeatedly travel along a straight line in the x direction. The results of their calculations for circular contact produced the interaction diagram shown in Figure 2 with axis given by P, in non-dimensional form, and f. The diagram is subdivided into a number of regions. In the Elastic region, purely elastic behaviour occurs and there is no plastic deformation, assuming the body was initially stress free. In the Elastic Shakedown region there will be some plastic strains during the first few traverses but subsequently the behaviour is purely elastic. In the Plastic Shakedown region local reverse cycles of plastic strains occur beneath the surface but there is no overall cyclic growth of strain. In the Ratchetting region cyclic growth of strain occurs. The region of primary interest in design is bounded by the line that surrounds the Elastic shakedown region and it is the direct determination of this boundary that forms the subject of this paper.

The approach of Ponter, Hearle and Johnson (1985) has subsequently been applied to pavement design problems by Boulbibane and Collins (2000) using a wider range of mechanisms of deformation. There is, however, an inherent weakness in the approach, the need to make assumptions about the particular classes of deformation modes that occur in these various cases.

In this paper we discuss a numerical method that seeks the mechanism, from within a class of mechanisms described by a finite element mesh, that minimises the

upper bound shakedown limit. The method, the Linear Matching Method , (Ponter and Engelhardt (2000), Chen and Ponter (2001), Ponter *et al* (2002)), is essentially a programming method that seeks mechanisms that produce a reducing sequence of upper bounds, converging to a least upper bound. At each iteration a linear problem is solved that matches the conditions of the non-linear problem in two respects. The material coefficients of the linear problem are chosen so that the linear material and the yield condition give rise to the same stress at the current estimate of the plastic strain rate history and the load is chosen as the current least upper bound. The basic idea, as an *ad hoc* method, has been applied in pressure vessel design for some years and developed by Mackenzie, Boyle *et al* (Mackenzie et al (1996), Boyle et al (1997)) and Seshadri and Mangalaramanan (1997) and most widely known as the Elastic Compensation method.

The Linear Matching method is here applied to the same class of rolling contact problems as discussed by Ponter, Hearle and Johnson (1985) with the following objectives; to develop a general method capable of solving rolling contact problems; to verify the correctless of the solution given by Ponter et al; to explore the effect of frictional force direction on the shakedown limit and to obtain shakedown limits for elliptical contact area.

2. The Upper Bound Shakedown Theorem

The material considered is assumed to be isotropic, elastic-perfectly plastic and satisfies the von Mises yield condition. The problem consists of a body *V* with boundary S, which experiences a history of cyclic load $\lambda P_i(x_j,t)$ on S_T (and possible a temperature history $\lambda\theta(x_j,t)$ within *V*). λ is a load parameter. The displacement rate $\dot{u}_i = 0$ is applied on S_u. Both S_T and S_u are complementary parts of the boundary S. The linear elastic solution to the problem is denoted by $\lambda\hat{\sigma}_{ij}$.

The upper bound shakedown theorem is expressed in terms of an incompressible and kinematically admissible strain rate history $\dot{\varepsilon}_{ij}^c$, which need not be compatible but associated with a compatible strain increment $\Delta\varepsilon_{ij}^c$ such that

$$\int_0^{\Delta t} \dot{\varepsilon}_{ij}^c dt = \Delta \varepsilon_{ij}^c \tag{1}$$

which in turn is associated with the corresponding displacement increment field Δu_i^c,

$$\Delta \varepsilon_{ij}^c = \frac{1}{2}\left(\frac{\partial \Delta u_i^c}{\partial x_j} + \frac{\partial \Delta u_j^c}{\partial x_i} \right) \tag{2}$$

In terms of the load history described above the upper bound shakedown limit is given by

$$\lambda_{UB} \int_V \int_0^{\Delta t} \left(\hat{\sigma}_{ij} \dot{\varepsilon}_{ij}^c \right) dt dV = \int_V \int_0^{\Delta t} \sigma_{ij}^c \dot{\varepsilon}_{ij}^c dt dV \tag{3}$$

where σ_{ij}^c is the stress at yield associated with $\dot{\varepsilon}_{ij}^c$ and $\hat{\sigma}_{ij}$ is the linear elastic solution associated with the load history P and θ. $\lambda_{UB} \geq \lambda_s$ is an upper bound to the shakedown load parameter λ_s. For the von Mises yield condition equation (3) can be simplified as

$$\lambda_{UB} = \frac{\int_V \int_0^{\Delta t} \sigma_y \bar{\dot{\varepsilon}} \left(\dot{\varepsilon}_{ij}^c \right) dt dV}{\int_V \int_0^{\Delta t} \left(\hat{\sigma}_{ij} \dot{\varepsilon}_{ij}^c \right) dt dV} \tag{4}$$

where $\bar{\dot{\varepsilon}} = \sqrt{\frac{2}{3} \dot{\varepsilon}_{ij} \dot{\varepsilon}_{ij}}$ is the effective strain rate and σ_y denotes the uniaxial yield stress. For a given load history, we seek the kinematically admissible strain rate history that minimises the upper bound (4) within a class of displacement fields described, for example, by a particular finite element mesh.

3. The Linear Matching Method

The general programming method described by Ponter and Engelhardt (2000) consists of defining a sequence of linear problems where the linear coefficients are chosen so they match the yield condition. For a von Mises yield condition the relevant linear material is incompressible with a shear modulus μ. A single step in the method

begins with a kinematically admissible history of plastic strain rate $\dot{\varepsilon}_{ij}^{i}$, in terms of which the following linear problem is posed for a new history $\dot{\varepsilon}_{ij}^{f}$;

$$\dot{\varepsilon}_{ij}^{f\prime} = \frac{1}{\mu}(\lambda_{ub}^{i}\hat{\sigma}_{ij} + \overline{\rho}_{ij}^{f})', \quad \dot{\varepsilon}_{kk}^{f} = 0, \text{ and } \mu = \frac{\sigma_y}{\bar{\dot{\varepsilon}}^{i}} \tag{5}$$

subject to the condition that $\dot{\varepsilon}_{ij}^{f}$ is also a kinematically admissible strain rate history and $\overline{\rho}_{ij}^{f}$ is a constant equilibrium residual stress field. The equation for μ comes from matching the linear material to the perfectly plastic material so that they both give the same effective stress corresponding to $\dot{\varepsilon}_{ij}^{i}$. Here $\dot{\varepsilon}_{ij}^{f\prime}$ refers to the deviator component of $\dot{\varepsilon}_{ij}^{f}$ and this notation is used throughout. Note that $\lambda = \lambda_{UB}^{i}$, the upper bound (4) corresponding to $\dot{\varepsilon}_{ij}^{i}$. Integration of (5) over the cycle of loading produces the following equation relating $\Delta\varepsilon_{ij}^{f\prime}$ and $\overline{\rho}_{ij}^{f\prime}$,

$$\Delta\varepsilon_{ij}^{f\prime} = \frac{1}{\overline{\mu}}\left(\overline{\rho}_{ij}^{\prime f} + \sigma_{ij}^{\prime in}\right) \tag{6}$$

$$\text{where } \sigma_{ij}^{\prime in} = \overline{\mu}\left\{\int_0^{\Delta t} \frac{1}{\mu(t)}\lambda_{UB}^{i}\hat{\sigma}_{ij}^{\prime}(t\ )dt\right\} \text{ and } \frac{1}{\overline{\mu}} = \int_0^{\Delta t}\frac{1}{\mu(t)}dt. \tag{7}$$

The solution to this incompressible linear problem yields a new upper bound λ_{UB}^{f} by substituting $\dot{\varepsilon}_{ij}^{f}$ into (4) which satisfies (Ponter and Engelhardt (2000)),

$$\lambda_{ij}^{f} \le \lambda_{ij}^{i} \tag{8}$$

with equality if and only if $\dot{\varepsilon}_{ij}^{f} \equiv \dot{\varepsilon}_{ij}^{i}$. Hence the repeated application of this algorithm produces a monotonically reducing sequence of upper bounds that converges to a minimum upper bound. A general discussion of the method has been given by Ponter *et al.* (2002). If the linear problems are solved using a finite element method then the sequence converges to the least upper bound associated with the finite element mesh. In this, very general, statement of the method the solution is an intrinsic property of the entire elastic stress history $\hat{\sigma}_{ij}$. There are many problems where it is possible to identify instants during the cycle when inelastic strains occur and the relationships (7) may be reduced to a finite sum with a predetermined number of terms, (Ponter and

Engelhardt (2000), Chen and Ponter (2001)). For rolling contact problems this is not generally the case and the integrals (7) need to be made over the entire elastic stress history.

4. Application of the Method to Rolling Contact Problems

The most common rolling contact problem consists of a body of infinite extent in a cartesian axis direction x. The body is then defined by its geometry shape in the orthogonal (y,z) plane. A rolling or sliding contacting body passes, quasi-statically, along a line of travel in the x direction. As a typical material element in each (y,z) cross section of the body experiences an identical history of elastic stress, any resultant deformation field will vary within a (y,z) plane but will be independent of x. Hence $\dot{\varepsilon}_{ij}^{c}$, $\Delta\varepsilon_{ij}^{c}$ and Δu_i^c are all independent of x and depend only on y and z. The history of linear elastic solution at a fixed material point x_i may be written in the general form;

$$\hat{\sigma}_{ij}(x_i,t) = \hat{\sigma}_{ij}(x+vt, y, z) \tag{9}$$

where v is the velocity of travel of the contacting body. A single cycle of loading for a material element in the plane $x=0$ consists of $-t_0 \le t \le t_0$ where t_0 is sufficient large for the elastic stress at $(\pm vt_0, y, z)$ to be negligibly small. In the following we apply these characteristics of the problem directly to the finite element solution method.

Although the upper bound (4) is expressed in terms of the entire history of the elastic stress, at each point in the (y,z) plane the contribution to the total accumulated strain $\Delta\varepsilon_{ij}^{c}$ usually occurs at one or two instants during the cycle when the extremes of the elastic stress history occurs. We descretise the problem by dividing up the cycle of loading into r-1 equal time intervals and hence r instants when plastic strains may potentially occur. The integral (1) becomes the finite sum;

$$\Delta\varepsilon_{ij}^{c} = \sum_{n=1}^{r} \Delta\varepsilon_{ij}^{n} \tag{10}$$

Hence the linear problem for a new kinematically admissible strain rate $\Delta\varepsilon_{ij}^{f}$ and a time constant residual stress field $\overline{\rho}_{ij}^{f}$ may be defined by (5) where

$$\sigma_{ij}'^{in} = \overline{\mu}\left\{\sum_{n=1}^{r}\frac{1}{\mu_n}\lambda\hat{\sigma}_{ij}'(t_n)\right\} \tag{11a}$$

and $$\frac{1}{\overline{\mu}} = \sum_{n=1}^{r}\frac{1}{\mu_n} \text{ where } \mu_n = \frac{\sigma_y}{\overline{\varepsilon}(\Delta\varepsilon_{ij}^{ni})} \tag{11b}$$

Convergence of the method with respect to r then consists of increasing the number of time intervals until there is a negligible change in the solution.

5. Implementation of the Method

A very significant advantage of the method comes from the ability to use standard commercial finite element codes that have the facility to allow the user to define the material behaviour. This has been done in the code ABAQUS (2000) of HKS Ltd using a method devised by Engelhardt (1999). Essential, ABAQUS carries out a conventional step-by-step analysis and, through the use of user routines, each increment is reinterpreted in terms of an iteration of the method.

The iteration step in ABAQUS is achieved by a user subroutine UMAT that allows material characteristics to be defined at each Gaussian integration point. Access to the output of each iteration is provided by a user subroutine URDFIL. The sequence of calculations is as follows:

1. For the first iteration, k=1, the linear elastic solution $\hat{\sigma}_{ij}(t_n)$ is evaluated for r instants of the load history at each Gauss point and we take, arbitrarily, $\mu_n^{\,1} = 1$. The elastic stress solutions $\hat{\sigma}_{ij}(t_n)$ may be generated by solving a linear elastic problem separately for the same mesh. In the following examples we use know analytic solutions.

2. For the (k+1) iteration we define:

$$\lambda^{k+1} = \lambda_{UB}^{k} \tag{12a}$$

$$\mu_n^{k+1} = \frac{\sigma_y}{\bar{\varepsilon}_n^k} \text{ where } \bar{\varepsilon}_n^k = \bar{\varepsilon}(\Delta\varepsilon_{ij}^{nk}) \tag{12b}$$

and
$$\frac{1}{\bar{\mu}^{k+1}} = \sum_{n=1}^{r} \frac{1}{\mu_n^{k+1}} \tag{12c}$$

From the calculated values of $\bar{\mu}^{k+1}$ we can obtain $[J]^{k+1}$, the Jacobian that relates increments of stress and strain in UMAT but reinterpreted as the relevant Jacobian for the linear problem of the iterative process. We define

$$\sigma_{ij}^{in\,k+1} = \bar{\mu}^{k+1}\left(\sum_{n=1}^{r} \frac{\lambda^{k+1}\hat{\sigma}_{ij}(t_n)}{\mu_n^{k+1}}\right) \tag{13}$$

The constant residual stress then can be calculated by the standard form required for input to UMAT,

$$\bar{\rho}_{ij}^{k+1} = [J]^{k+1}\Delta\varepsilon_{ij}^{k+1} - \sigma_{ij}^{in\,k+1} \tag{14}$$

The strain increments associated with the r instants of the load history are given by

$$\Delta\varepsilon_{ij}^{n(k+1)} = [C]_n^{k+1}\left(\bar{\rho}_{ij}^{k+1} + \hat{\sigma}_{ij}^{k+1}(t_n)\right) \tag{15}$$

where $[C]_n^{k+1}$ is the stiffness matrix derived from μ_n^{k+1}.

And further we can calculate the effective strain for each strain increments $\Delta\varepsilon_{ij}^{n(k+1)}$, $\bar{\varepsilon}_n^{k+1}$, and the integrands of the upper bound, $\left(\sigma_y \sum_{n=1}^{r} \bar{\varepsilon}_n^{k+1}\right)$ and $\left(\sum_{n=1}^{r} \Delta\varepsilon_{ij}^{n(k+1)}\hat{\sigma}_{ij}(t_n)\right)$, for each Gauss integration point in the structure.

3. From the energy output files of ABAQUS, the volume integrals $\int_V \left(\sigma_y \sum_{n=1}^{r} \bar{\varepsilon}_n^{k+1}\right) dV$ and $\int_V \left(\sum_{n=1}^{r} \Delta\varepsilon_{ij}^{n(k+1)}\hat{\sigma}_{ij}(t_n)\right) dV$ can be obtained and thus the load multiplier

$$\lambda_{UB}^{k+1} = \frac{\int_V \left(\sigma_y \sum_{n=1}^{r} \bar{\varepsilon}_n^{k+1}\right) dV}{\int_V \left(\sum_{n=1}^{r} \dot{\varepsilon}_{ij}^{n(k+1)}\hat{\sigma}_{ij}(t_n)\right) dV} \tag{16}$$

may be determined. In this way an exact implementation of the iterative method may be obtained. Implementation errors only occur in the integrations involved in the

evaluation of the element and global stiffness matrices for the linear problem (13). This is achieved through standard Gaussian integration with a number a Gauss points that would yield exact integrals if the Jacobian $[J]$ were constant throughout an element. As $[J]$ is proportional to $\bar{\mu}$ which varies from Gauss point to Gauss point, there is an integration error. This observation applies equally to the evaluation of the volume integrals that make up the upper bound. Experience with the method indicates that this error is not significant if a sufficiently fine mesh is adopted. In all other respects the implementation is exact.

6. The Finite Element model and loading condition for rolling and sliding contacts

The above numerical procedure has been used to solve the rolling and sliding contact problem discussed by Ponter, Hearle and Johnson (1985). We consider an elastic-perfectly-plastic half-space over whose surface a prescribed traction is repeatedly traversed. In the general case, free rolling contact will be represented by a Hertzian distribution of pressure,

$$p(x,y) = p_0[1-(x/a)^2-(y/b)^2]^{1/2} \qquad (17a)$$

acting on the elliptical area of semi-axes a and b where, here, x=y=0 corresponds to the centre of contact area. When sliding accompanies rolling an additional shear traction occurs,

$$q(x,y) = fp_0[1-(x/a)^2-(y/b)^2]^{1/2} \qquad (17b)$$

where f is the coefficient of friction and will be taken to act in the direction of travel when $a \neq b$. Analytic linear elastic solution for the general elliptic case have been given by Sackfield and Hills (1983) and by Hamilton (1983) for a circular contact region.

First we consider a circular contact problem where the frictional contact stresses may act at an angle to the direction of travel. Accepting the simplifications introduced by Hertz and Mindlin, the boundary stresses are given within a circle of radius a by Hamilton (1983):

$$\sigma_z = \frac{3P}{2\pi a^3}\left(a^2 - x^2 - y^2\right)^{1/2} \tag{18a}$$

$$\tau_{zx} = \frac{3F}{2\pi a^3}\left(a^2 - x^2 - y^2\right)^{1/2} \tag{18b}$$

$$\tau_{zy} = \frac{3Q}{2\pi a^3}\left(a^2 - x^2 - y^2\right)^{1/2} \tag{18c}$$

where $x^2 + y^2 \le a^2$. Here $P = 2/3\, p_0$ is the total normal load in the z-direction, F is the total tangential force in the y-direction, perpendicular to the direction of travel, and Q is the total frictional force in the direction of travel, the x-direction as shown in Figure 3. All the boundary stresses outside the circle of contact are zero. A generalized coefficient of friction f and the angle θ between the x- direction and the resultant frictional force are given by

$$f = \frac{\sqrt{F^2 + Q^2}}{P}, \qquad \tan\theta = \frac{F}{Q} \tag{19}$$

The radius of the circle of contact a is given by the well known Hertzian expression:

$$a = \left\{\frac{3\pi PR}{4}\left[\frac{1-\nu^2}{\pi E}\right]\right\}^{1/3} \tag{20}$$

where E and ν are Young's modulus and Poisson's ratio of the half plane and R is the radius of curvature of the contacting sphere, assumed rigid. The analytical elastic stress field in the half-space for circular contact under the combined action of P, Q and F is obtained by supposition of the solution for the frictional force in the direction of travel (given by Hamilton (1984)) and the same solution rotated by 90° about the z axis.

Considering the property of the half-space, we take a cuboid with the size of $40a \times 20a \times 2a$, discretize by 3-D 8-node isoparametric finite element. All cross-sections of the half-space along x-axis experience the same distribution of displacement, which is therefore independent of x. In principle a solution could be obtained by using a mesh with only a single element in the x direction, but we find the best solutions are obtained by allowing a significant number of elements in the x direction. We then impose the boundary condition on the two faces x=constant that the nodal displacements at nodes with the same (y, z) co-ordinates have the same

displacements. Such linked node boundary conditions are a standard feature of ABAQUS. Zero-displacement constraints are imposed on the remaining three surfaces except the top surface z=0. The detailed mesh arrangements on three faces of the model are shown in Figure 4-6, respectively. The total number of the element is up to 19200. It can be seen in these figures that in order to optimise the numerical efficiency and accuracy, the finite element mesh has been chosen to make the distribution of the elements near the contact area more dense than those distributed in other parts of the structure. Detailed discussion about the effects on the results of the mesh geometry and the number of time instants r during the material element loading history will be presented later. The total number of the load instance in the computation is up to 42.

7. Numerical results for rolling and sliding point contacts

Converged solutions for a circular contact region are presented in Figure 7 in the form of an interaction diagram where $k = \sqrt{3}\sigma_y$ denotes the shear yield stress. Solutions for $\theta = 0$ may be directly compared with the solution of Ponter, Hearle and Johnson (1985) reproduced here as Figure 2. For $f \le 0.15$ the shakedown limit is a reserve plasticity limit and the numerical solution reproduce the solution of Figure 2 very accurately. In Figure 11 the optimal mechanism is shown for $f = 0.1$ as a contour plot of constant $\bar{\varepsilon}(\Delta\varepsilon_{ij}^k)$. The strain is concentrated at a single point corresponding to the maximum variation in effective stress in the elastic solution where the reverse plasticity mechanism occurs. For $f \ge 0.15$ the numerical solutions indicate that a global ratchet mechanism is activated, similar in form to that assumed by Ponter *et al.*. For $f = 0.2$ the numerical solutions are slightly below the Ponter solution but lies slightly above for $f = 0.6$. The optimal mechanism for $f = 0.25$ is shown in Figure 12. The type of mechanism assumed by Ponter et al where deformation is confined to a slip band surrounding the loaded surface is clearly reproduced although there is a distinct gradient of strain, produced partially by the nature of the finite element displacement fields and partially by the averaging process involved in the standard ABAQUS plotting routines. Figure 13 shows strain contours for $f = 0.6$ showing the strain concentrated at the surface, again in accordance with

Ponter *et al*.. The general nature of the Ponter solutions is clearly correct although the assumption that deformation only occurs in the direction of travel is clearly an approximation for intermediate values of f. However, the displacement fields generated by the finite element approximation cannot easily reproduce the slip surfaces assumed in the Ponter solution that are clearly optimal for higher values of f when the ratchet mechanism coincides with the surface. Figures 14, 15 and 16 show plots for Q=0, i.e. the frictional force acting in a direction perpendicular to the direction of rolling acting to the left. The nature of the mechanism is similar to the F=0 case, except that the distribution is biased towards to directional of the frictional force involving deformation in that direction. Figures 17, 18 and 19 shown strain plots for intermediate cases showing, again, similar behaviour.

For the case of an elliptic contact area, elastic solutions given by Sackfields and Hills (1983) only include the case where the frictional force acts in the direction of travel. A complete set of optimal solutions for $0 \le f \le 0.4$ and $0.25 \le b/a \le 4$ are shown in Figure 8 where the load is divide by the area of the ellipse. The same data is shown in Figure 9 in the form of contours of constant f.

For large b/a the solutions would be expected to converge towards the line contact solution. The analytic solution, based upon the line contact elastic solution (Johnson 1996), is shown for comparison and lies below but close to the solutions for $b/a = 4$. There are, however distinct differences. For line contact and $f = 0$, a reverse plasticity mechanism and ratcheting below the surface yield identical shakedown loads. For $f \ge 0$, the subsurface ratcheting mechanism yields a lower shakedown load. For $f \ge 0.34$ the ratchet mechanism lies at the surface. For $b/a = 4$ a reverse plasticity solution dominates for a significant range of f before a subsurface mechanism dominates. By inspection of the strain plots for the optimal mechanisms it is possible to identify regions of the interaction diagram where the three principal mechanism types operate, labeled as RP for reverse plasticity, R for subsurface ratchet mechanism and SR for surface ratchet mechanism. The boundary between these regions are shown in Figure 8; these boundaries are necessarily approximate. For large b/a the solution for $f = 0$ may be expected to converge to either the limit load solution or the reverse plasticity solution for the indentation problem. The lesser of these, the limit load solution assumed to be the Prandl solution,

is shown as the case $b/a \to 0$. This solution is significantly greater than the solution for $b/a = 0.25$.

For all values of b/a the shakedown limits are near identical for $f = 0.4$ where the mechanism is localized ratcheting on the surface.

8. Numerical Issues – Factors that affect the accuracies of solutions

8.1 The effects of mesh arrangement

The solutions discussed above were obtained for a finite element mesh and set of loading instants chosen as result of a process of optimization, described below. The convergence of the upper bound with iterations for three finite element models with differing mesh arrangement is shown Figure 10 with details in Table 1. For all three models, the total numbers of the elements exceeds 1000. However the final converged shakedown limit multipliers λ differ significantly. Model 1, which yields the poorest result, differs from Models 2 and 3 by having only half the element number in the x-direction, indicating the need for a significant number of elements in the direction of travel. The chosen Model 3, for the solutions described above, also involves a greater number of elements in the transverse y-direction. The rate of convergence in all three cases is similar and a converged solution for λ was obtained in 30-70 iterations assuming no change in the 7^{th} significant figure for two consecutive iterations.

8.2 The effects of the number of load instance

Table 2 shows the variations of the shakedown multiplier, iteration number and total CPU time with the number of load instants r. The optimal upper bound reduces with r and reaches a stable value when r approaches 40. The value of $r = 42$ was used in the solutions described above as higher values increased the CPU time without significant change in the solution. It is evident from these studies that careful optimization of the mesh geometry and number of load instants have a significant effect on converged solutions

9. Conclusions

The paper describes a powerful and efficient numerical method for the evaluation of shakedown limits for rolling and sliding point contact problem based upon the Linear Matching Method, interpreted as a non-linear programming method for which strict convergence proofs exist.

The analytic linear elastic solutions for elliptical and circular Hertzian contact problems provided by Sackfield and Hills (1983), and Hamilton (1983) form the basis for a series of calculations of least upper bound shakedown limits for the rolling contact of a half space for both a circular and an elliptic contact region. For accurate solutions we show that it is necessary to optimise the finite element mesh and the number of time instants during the loading sequence.

For a circular contact area and a frictional force in the direction of travel, direct comparison was made with the semi- analytic solutions of Ponter, Hearle and Johnson (1986). The numerical solutions generally agree with these solutions. However, it is clear that the kinematic assumption of the Ponter, Hearle and Johnson solutions, that deformation only takes place in the direction of travel, is not always strictly correct but provides a very good first approximation when the frictional force is in the direction of travel. The numerical solutions produced optimal mechanisms associated with the shakedown limit that were very similar in form to those assumed by Ponter *et al.*. New solutions are presented where the direction of the frictional loading forms an angle to the direction of rolling. In all such cases the shakedown limit was increased when normalised with respect to the friction coefficient, the greatest increase occurring when the frictional force acts perpendicular to the direction of travel.

Solutions are then presented for the case of an elliptic contact area and, again, with the frictional force in the direction of travel. These solutions show that the general character of the ratchet mechanisms is the same as the circular contact case. It is possible to describe the range of frictional coefficient f and ratio of principal axis b/a for which reverse plasticity, subsurface ratchet mechanisms and surface ratchet mechanisms occur. When normalised with respect the average normal pressure over the contact area, the shakedown limit monotonically decreases with b/a. For the largest value of $b/a = 4$ the limit is very close to the line contact solution, the limit as $b/a \to \infty$ and this solution forms a lower bound for all solutions. The variation with

b/a decreases with increasing f. For $f = 0.4$ the shakedown limit is very insensitive to b/a and the ratchet mechanism involves very localised plastic deformation at the surface.

The solutions presented in this paper demonstrate that it is possible to generate accurate shakedown solutions numerically for rolling contact problems using, essentially, standard finite element methods. Such solutions, when drawn together into interaction diagrams, provide broad insight into the factors that influence the onset of plastic strain growth and, therefore, are of use in design.

Acknowledgements

The HC and ARSP gratefully acknowledge the support of the Engineering and Physical Sciences Research Council of the United Kingdom during the course of this work. Thanks are due to the University of Bari for support for GS during a student project period at Leicester University. Thanks are due to Alex Savoury of the Department of Engineering, Leicester University, for the analytic solution for line contact shown in Figure 8.

References

ABAQUS, User's Manual 2001 HKS Ltd, Providence, Rhode Island, USA, Version 6.2.

Boyle, J. T., Hamilton, R., Shi, J. and Mackenzie, D. 1997 *J. Pressure Vessel Tech*, **119**, 236-242.

Boulbibane M and Collins I. 2000 *J. Geotechnical and Geoenvironmental Engineering* , ASCE, **126**, No 1, 50-59.

Chen H. F. & Ponter A.R.S. 2001 *International Journal of Pressure Vessels and Piping*, **78**(6), 443-451.

Engelhardt, M. 1999 PhD thesis, University of Leicester.

Hamilton, G.M. 1983 *Proc. Instn. Mech. Engrs.*, **197C**, 53-59.

Johnson K.L. 1985 Contact Mechanics, Cambridge University Press

Mackenzie, D., Boyle, J. T., Hamilton, and R. & Shi, J	1996	*Proceedings of the 1996* ASME *PVP Conference*, **338**, 203-208.
Ponter, A.R.S., Hearle, A.D. and Johnson, K.L.	1985	*J. Mech. Phys. Solids*, **33**(4), 339-362.
Ponter A. R. S. & Engelhardt, M.	2000	*European Journal of Mechanics, A/Solids*, **19,** 423-445.
Ponter, A.R.S.; Chen, H. Boulbibane, M. and Habibullah M.	2002	Proceedings of the Fifth World Congress on Computational Mechanics (WCCM V), Vienna, Austria, Editors: Mang, H.A.; Rammerstorfer, F.G.; Eberhardsteiner, J., Publisher: Vienna University of Technology, Austria, ISBN 3-9501554-0-6, 21 pages, http://wccm.tuwien.ac.at (available for downloading until 2008)
Sackfield, A. and Hills, D. A.	1983	Journal of Strain Analysis, **18**, 101-105.
Seshadri, R. and Mangalaramanan, S. P.	1997	*International Journal of Pressure Vessels & Piping*, **71**, 93-106.

Model	No. of element along y direction	No. of element along x direction	No. of element along z direction	No. of element in the model
Model 1	36	10	30	10800
Model 2	40	20	20	16000
Model 3	48	20	20	19600

Table 1. The mesh arrangement in the different finite element models discussed in Figure 10. ($Q = 0.15P$, $F = 0.45P$, $f = 0.474$)

No. of load instants	Converged upper bound λ	Iterations to convergence	Total CPU time (seconds)
4	3.6863	45	18858
12	3.3771	50	21017
22	3.3327	64	26832
42	3.3267	71	30158

Table 2. The effects of the number of load instants on the shakedown limit

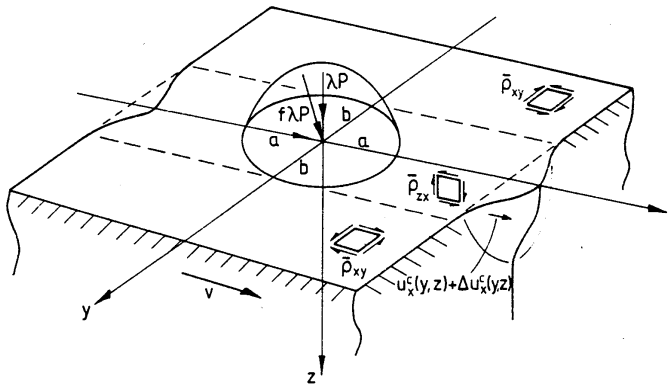

Mode of deformation in point contact: displacement of a surface segment $u_x^c(y, z)$.

Figure 1. Rolling contact problem considered by Ponter, Hearle and Johnson (1985)

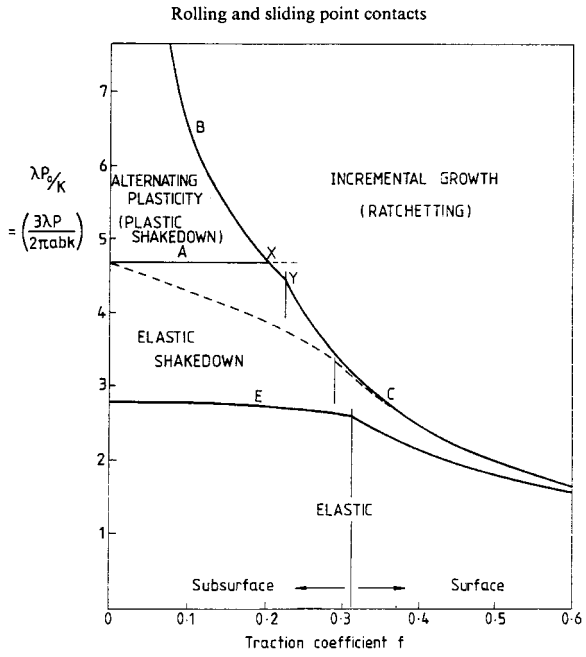

Figure 2. Shakedown and Ratchet Boundary diagram for the Hertzian rolling circular contact problem (a=b); solution given by Ponter, Hearle and Johnson (1985)

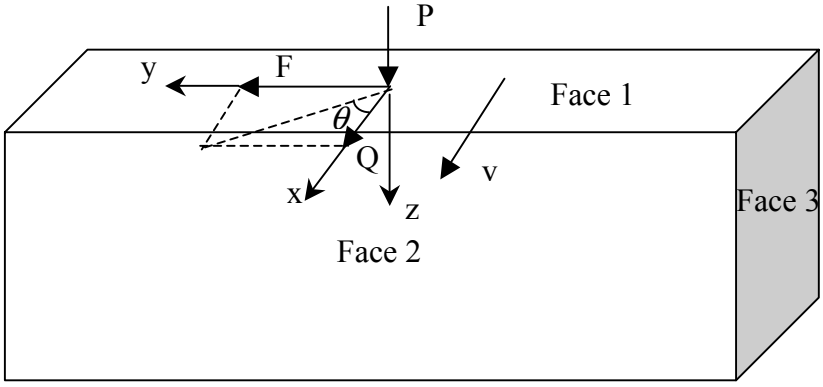

Figure 3. The model for point contact; the x axis is the direction of rolling

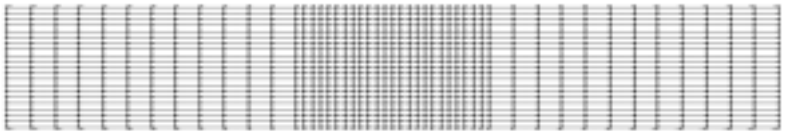

Figure 4. The mesh arrangement in face 1 of model 3 (48x20elements)

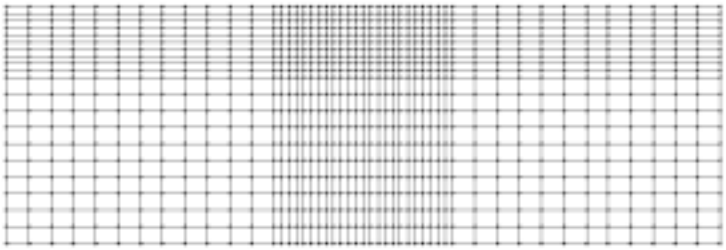

Figure 5. The mesh arrangement in face 2 of model 3 (48x20elements)

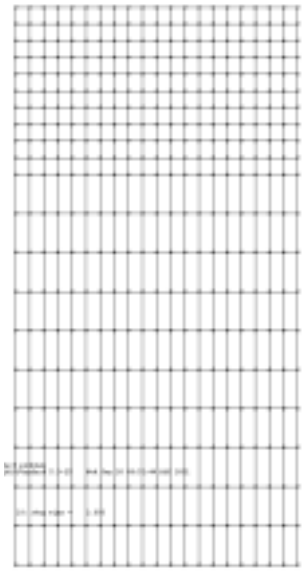

Figure 6. The mesh arrangement in face 3 of model 3 (20x20)

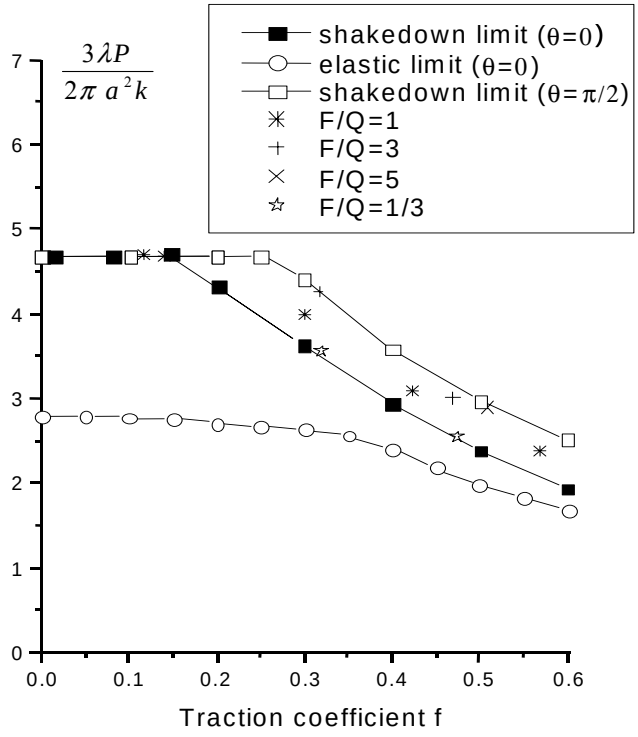

Figure 7. Shakedown and elastic limit of a circular loaded region for different normal and tangential loads

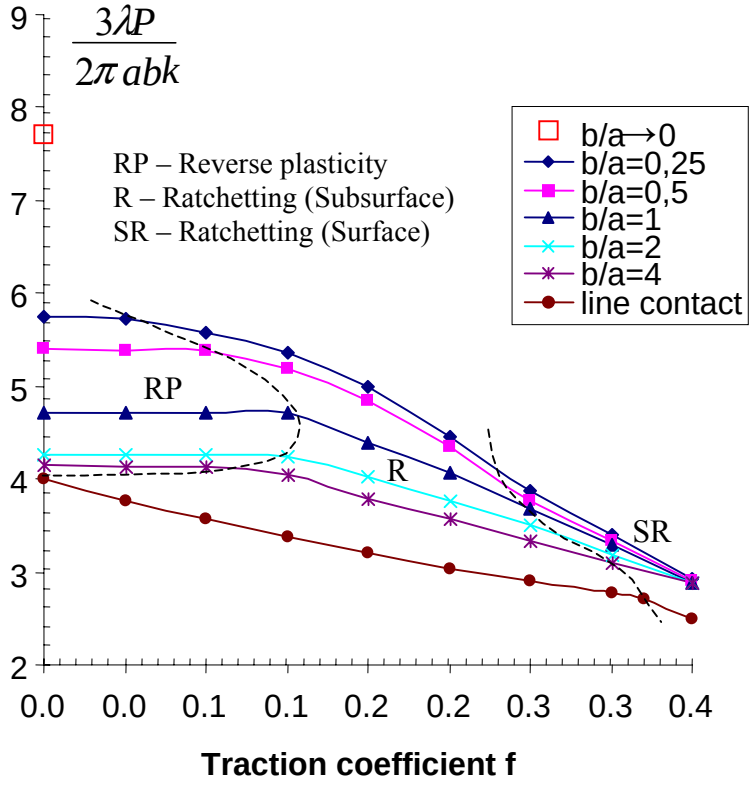

Figure 8. Shakedown limit of an elliptical loaded region for different normal and tangential loads ($\theta = 0$)

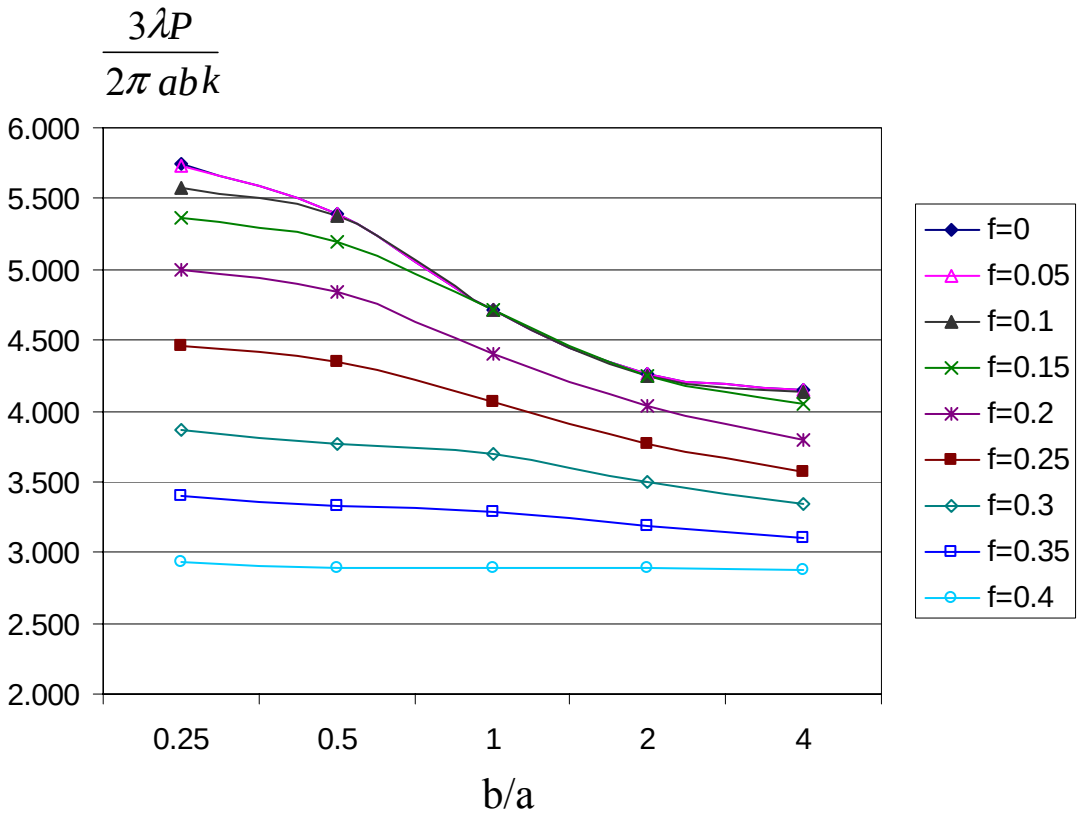

Figure 9. Variation of Shakedown limits with shape of loaded ellipse (b/a) for different normal and tangential loads ($\theta = 0$)

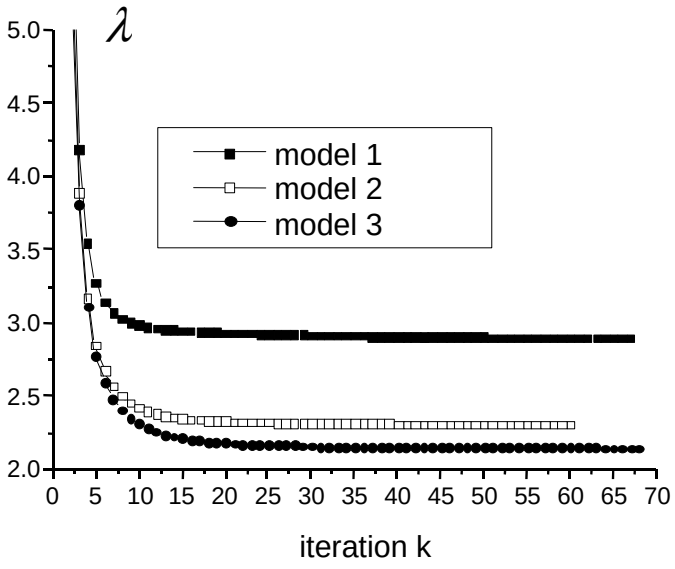

Figure 10. The convergence conditions for the three finite element models listed in Table 1

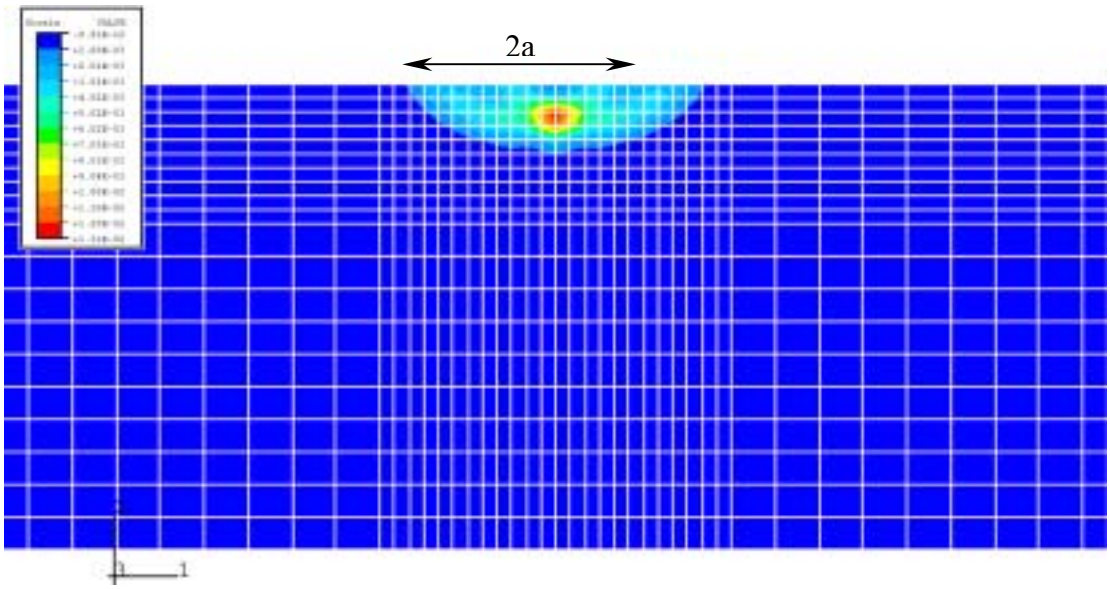

Figure 11. Contours of constant von Mises effective strain for the convergent mechanism; frictional force in direction of travel,
F=0, $a = b$, $f = 0.1$

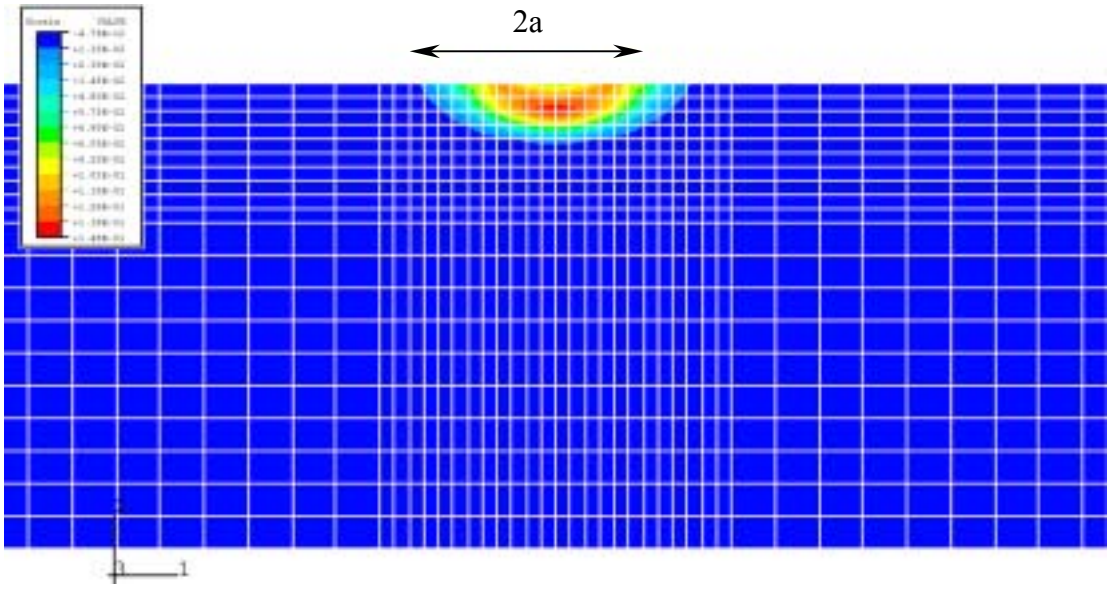

Figure 12. Contours of constant von Mises effective strain for the convergent mechanism; frictional force in direction of travel,
F=0, $a = b$, $f = 0.25$

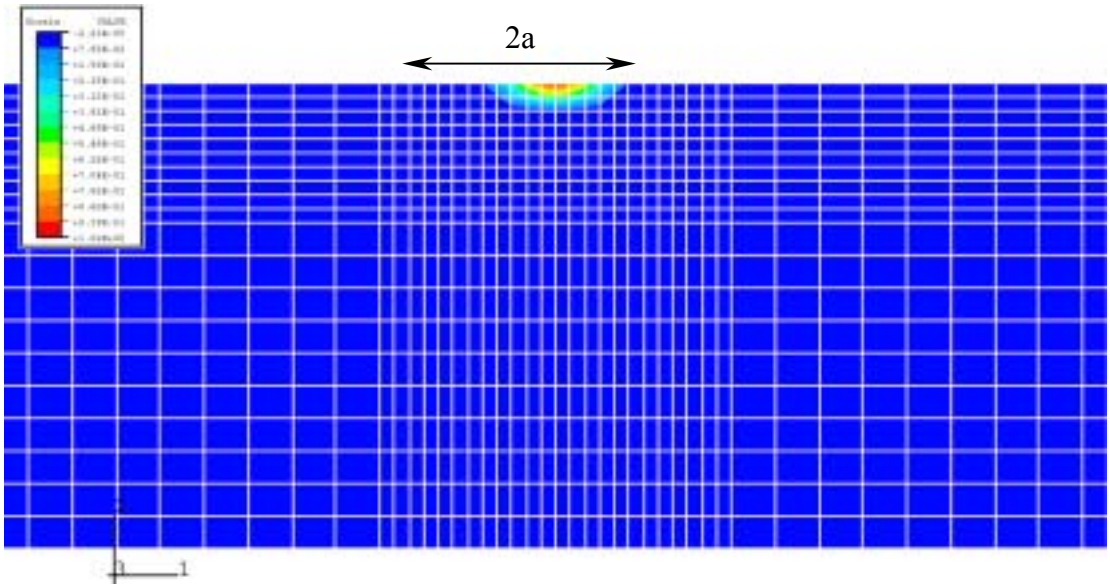

Figure 13. Contours of constant von Mises effective strain for the convergent mechanism; frictional force in direction of travel,
F=0, $a = b$, $f = 0.6$

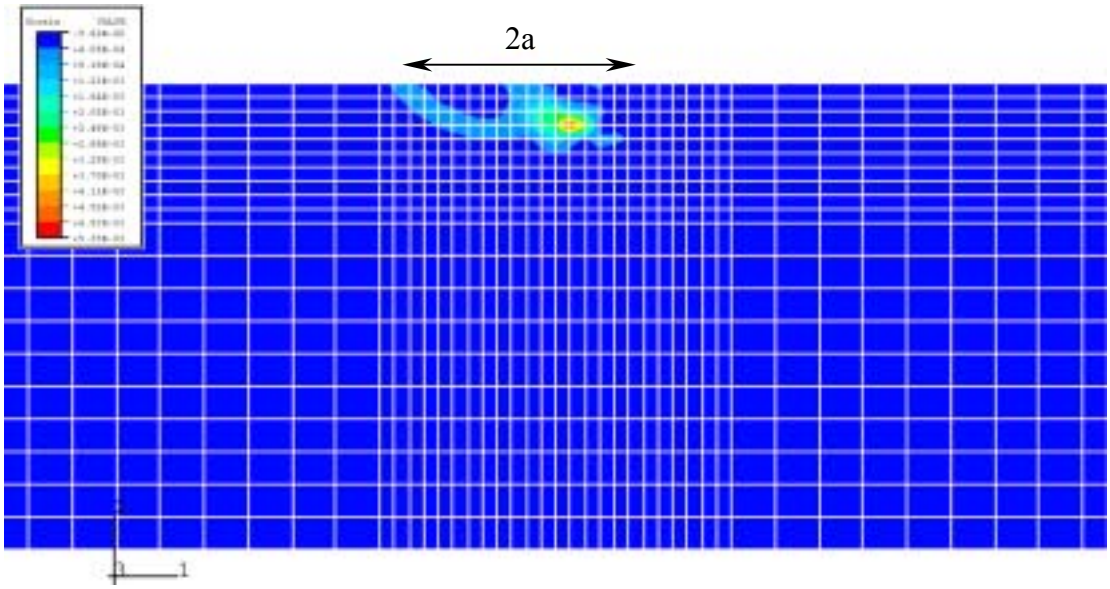

Figure 14. Contours of constant von Mises effective strain for the convergent mechanism; frictional force perpendicular to the direction of travel,
Q=0, $a = b$, $f = 0.1$

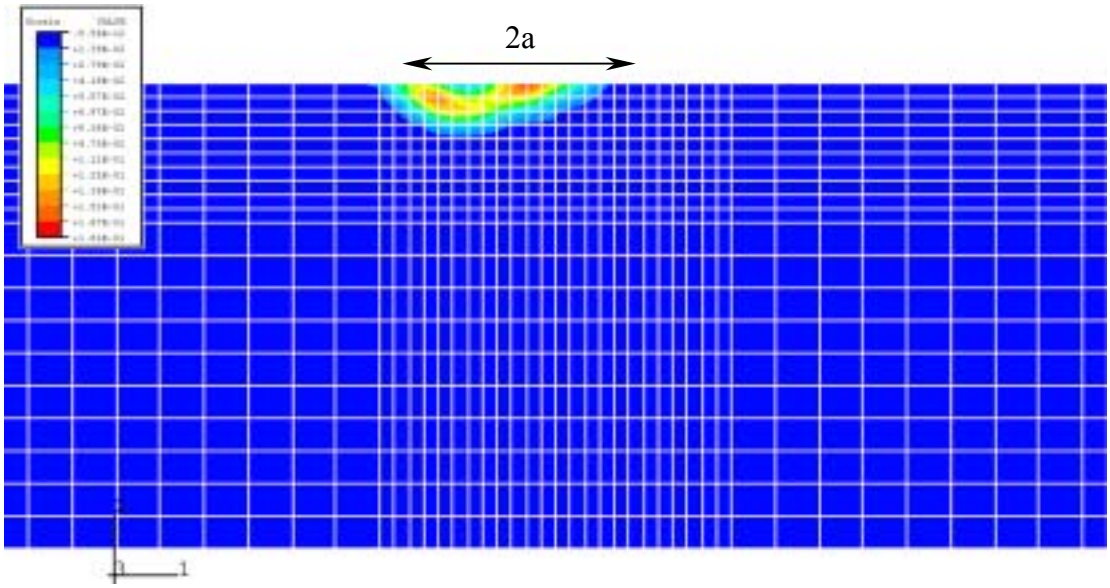

Figure 15. Contours of constant von Mises effective strain for the convergent mechanism; frictional force perpendicular to the direction of travel,
Q=0, $a = b$, $f = 0.25$

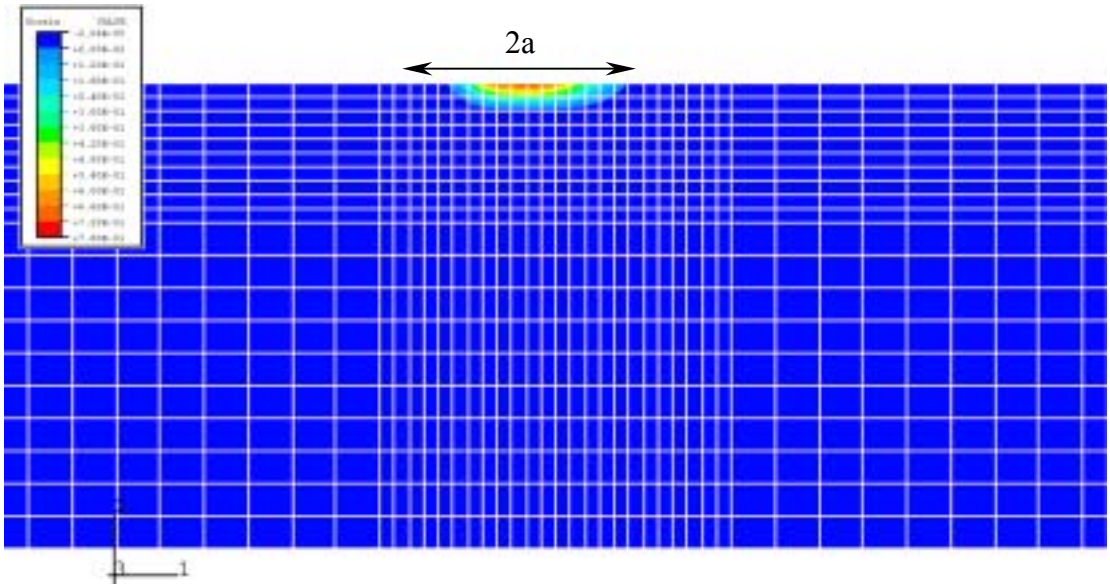

Figure 16. Contours of constant von Mises effective strain for the convergent mechanism; frictional force perpendicular to the direction of travel,
Q=0, $a = b$, $f = 0.6$

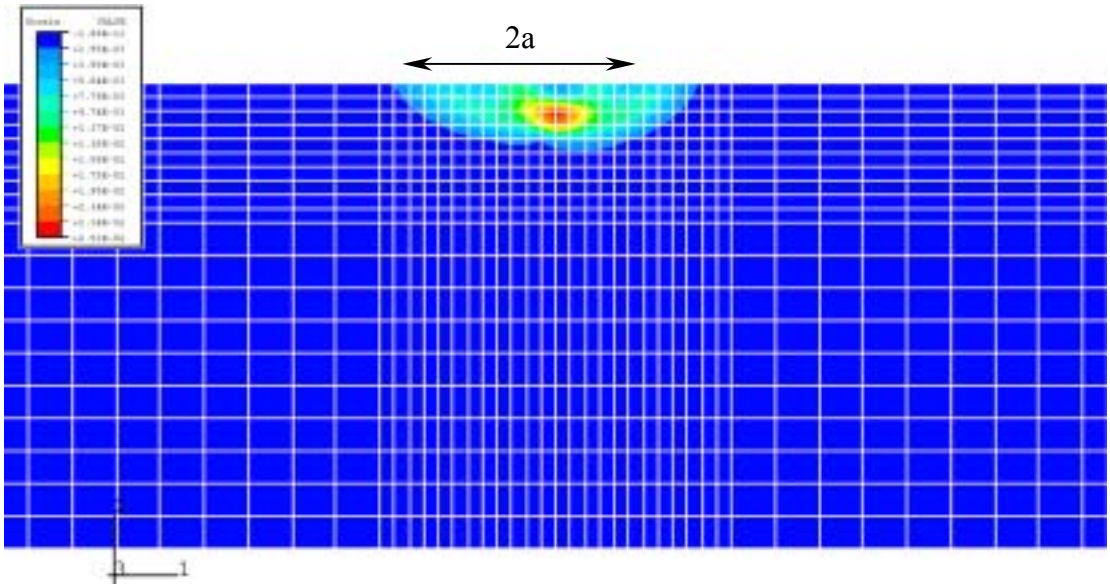

Figure 17. Contours of constant von Mises effective strain for the convergent mechanism; frictional force at $\theta = 45^{\circ}$ to the direction of travel, $a = b$, $f = 0.1$

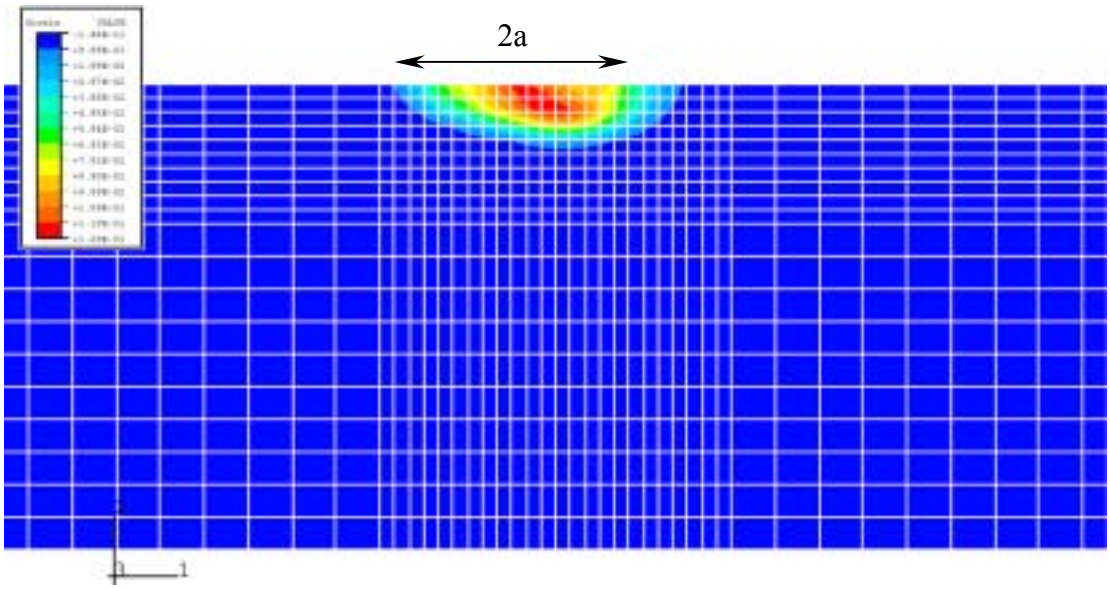

Figure 18 Contours of constant von Mises effective strain for the convergent mechanism; frictional force at $\theta = 45^{\circ}$ to the direction of travel, $a = b$, $f = 0.18$

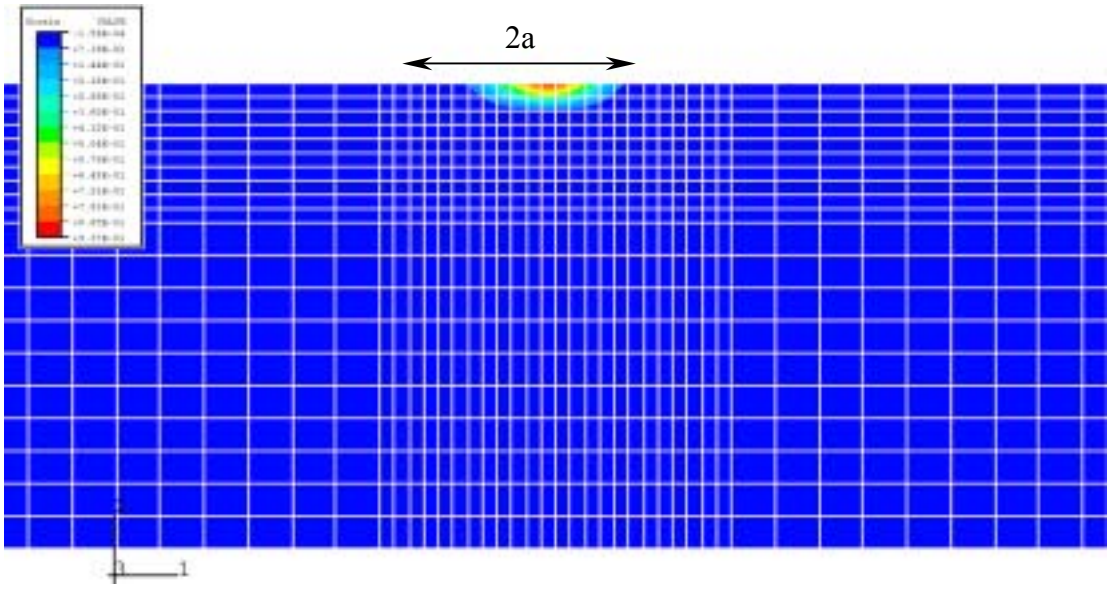

Figure 19. Contours of constant von Mises effective strain for the convergent mechanism; frictional force at $\theta = 45^{\circ}$ to the direction of travel, $a = b$, $f = 0.4$